Proceedings of the ASME 2010 3rd Joint US-European Fluids Engineering Summer Meeting and 8th International Conference on Nanochannels, Microchannels, and Minichannels
FEDSM-ICNMM2010
August 1-5, 2010, Montreal, Canada

FEDSM-ICNMM2010-30176

Nanofluidics meets Plasmonics: Flow-Through Surface-Based Sensing

C. Escobedo
Department of Mechanical Engineering,
University of Victoria

A.G. Brolo
Department of Chemistry,
University of Victoria

R. Gordon
Department of Electrical and Computer Engineering, University of Victoria

D. Sinton †
Department of Mechanical Engineering,
University of Victoria,
Victoria, BC, V8W 2Y2,
Canada

ABSTRACT

Nanostructures exhibit both nanofluidic and nanophotonic phenomena that can be exploited in sensing applications. In the case of nanohole arrays, the role of surface plasmons on resonant transmission motivates their application as surface-based biosensors. Research to date, however, has focused on dead-ended (or 'blind') holes, and therefore failed to harness the benefits of nanoconfined transport combined with plasmonic sensing. A flow-through nanohole array format presented here enables biomarker sieving and rapid transport of reactants to the sensing surface. Proof of concept operation is demonstrated and compared with previous methods. The various transport mechanisms are characterized with the aim to utilize the metallic plasmonic nanostructure as an active element in concentrating as well as detecting analytes.

The invited presentation will provide an overview of all our experimental, computational and analytical work in this area. This paper is focused on the analysis and evaluation of flow-through nanohole arrays for analyte sensing.

1. INTRODUCTION

Metallic films with ordered arrays of nanoholes exhibit surface plasmon resonance (SPR) that facilitates enhanced optical transmission through the holes [1-3]. The influence of the near-surface refractive index on the resulting transmission has been utilized for sensing applications [4, 5], and it has been established that the in-hole surface is the active sensing surface [6].

We recently demonstrated flow-through operation of nanohole array based sensors, schematically shown in Figure 1 [7]. Operating in flow-through mode, nanohole arrays have the potential to serve as analyte sieves: a capacity that is unique among surface based optofluidic sensors.

In this work, the sieving action (or collection efficiency) of flow-through nanohole arrays is quantified an characterized. The range of applicability of flow-through nanohole based sensor is established as a function of analyte diffusivity and the characteristic timescale of the binding kinetics. Scaling analyses are presented in the following section, followed by simulations.

2. THEORETICAL BACKGROUND AND SIMULATIONS

At low Reynolds numbers, characteristic of both microfluidic and nanofluidic flows, the motion of a Newtonian incompressible fluid is governed by the simplified Navier-Stokes and the continuity equations as follows

$$0 = -\nabla p + \mu \nabla^2 \vec{u} \quad (1)$$

$$\nabla \cdot \vec{u} = 0 \quad (2)$$

where ρ is the fluid density, t is the time, $\vec{u}$ is the local flow velocity, μ is the fluid viscosity and p is the local pressure in the fluid.

The systems simulated in this work assume unidirectional pressure-driven flow in thetwo 2-D domains, shown in Figure 2. The systems of interest are a microchannel with a surface based sensor (Figure 3a-left), and a similarly sized microchannel with a flow-through nanohole arrays sensor (Figure 3a-right). The microchannel domain, shown in Figure 2a, has a cross-section with 200 μm in width and 100 μm in height. The nanohole array consists of a square array of 40_x 40 holes of 260 nm diameter, 200 nm in length. The 2D rectangular geometry is typical of traditional SPR microsensors [8].

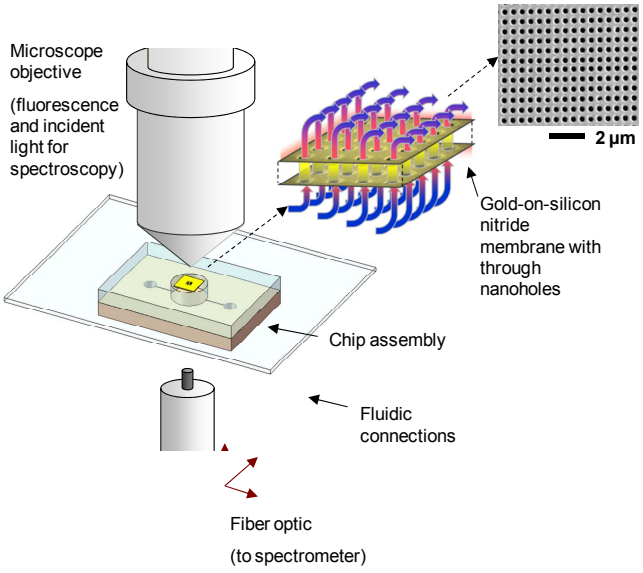

Figure 1. Schematic of the flow-through nanohole array concept and optical and fluidic test setup employed for both fluorescence tests and transmission spectroscopy.

The 2D axisymmetric geometry is typical of nanohole arrays milled through a composite layer of gold on silicon nitride [5]. In both cases fully developed laminar flow is described by a parabola defined by

$$\vec{u}(y) = U_{max}\left[1 - \frac{\left(y-\frac{H}{2}\right)^2}{\frac{H}{2}}\right] \quad (3)$$

where U_{max} is the velocity at the center of the channel and H is the characteristic dimension of the channel (channel width in the rectangular case and hole diameter in the nanohole case).

The rate of change of surface concentration $c_S(t)$ of analyte absorbed to the sensing surface, assuming first-order Langmuir kinetics [9], can be described by

$$\frac{\partial c_S}{\partial t} = D_S\nabla^2 c_S + k_{on}c_0(b_0 - c_S) - k_{off}c_S \quad (4)$$

where D_S is the diffusion coefficient of antigen-antibody complexes at the surface, c_0 is the bulk concentration, k_{on} is the adsorption constant, k_{off} is the desorption constant and b_0 is the total surface concentration of active potential binding sites.

In a reaction limited scenario, an analytical expression [10-13] for the surface concentration of adsorbed species can be obtained as follows

$$c_S(t) = \frac{b_0c_0k_{off}}{k_{on}c_0+k_{off}}\left(1 - e^{-(c_0k_{on}+k_{off})t}\right). \quad (5)$$

If the concentration of the bulk liquid is higher than the dissociation constant $K_D=k_{off}/k_{on}$ the surface concentration of adsorbed species at equilibrium is given by

$$c_S^{eq} = \frac{b_0c_0k_{off}}{k_{on}c_0+k_{off}} \quad (6)$$

And the time scale required for the sensor to equilibrate at this concentration is given by the second part of equation 5 [14] as follows

$$\tau = (c_0k_{on} + k_{off})^{-1} \quad (7)$$

In terms of nanoplasmonic sensing, this is the time required to achieve the maximum signal change which can be detected as means of light intensity or peak-shift in the transmission spectrum as reported previously [7].

The advection-diffusion species transport is governed by the following PDE

$$\frac{\partial c}{\partial t} = Diff\nabla^2 c - \vec{u}\cdot\nabla c \quad (8)$$

where c is the bulk concentration, *Diff* is the diffusion coefficient of the reacting species.

The coupling between the 2-D mass balance in the bulk and the 1-D concentration at the surface is achieved as a boundary condition in equation 1 at the sensing surface as follows

$$\vec{n}\cdot(c\vec{u} - D_S\nabla c_S) = -k_{on}c(b_0 - c_S) + k_{off}c_S$$

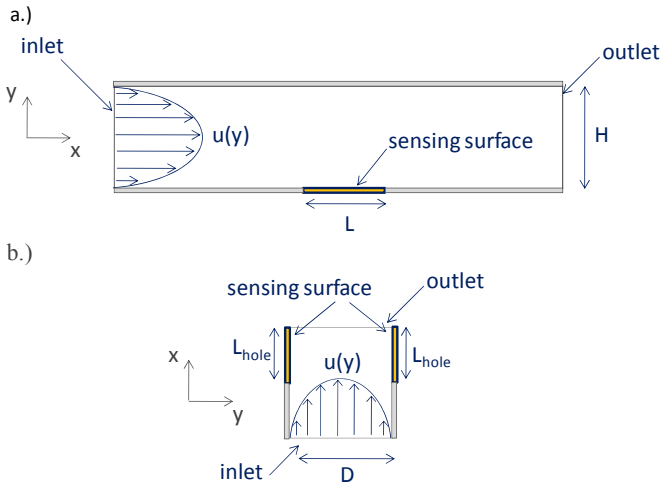

Figure 2. Schematic of a) the microchannel (not in scale) and b) the nanohole (not in scale) geometries used in the mass transport and reaction kinetics models

The boundary conditions in the rest of the model are

$c=c_0$	at the inlet
$\vec{n}\cdot(c\vec{u}-Diff\nabla c)=\vec{n}\cdot c\vec{u}$	at the outlet
$\vec{n}\cdot(c\vec{u}-Diff\nabla c)=0$	all other boundaries

The model described above was employed in both the scaling analysis and computational analysis. The computational analysis was performed in COMSOL Multiphysics (COMSOL, Sweden).

4. RESULTS AND DISCUSSION

In order to quantify and characterize the sieving action (or collection efficiency) of flow-through nanohole arrays, a scaling analysis is presented below, followed by simulations results. The two cases analyzed here are a planar SPR sensor in a microchannel, and a flow-through nanohole array of equivalent active area, as shown side-by-side in Figure 2a. Both the in-channel SPR sensor and the flow-through nanohole array are given an equivalent flow rate of an analyte solution.

The first case is the microfluidic SPR sensor with a sensing area of square geometry and side length L (L ~ 100 μm would be typical) located in a square channel of matching width, L, and height, H. A flowrate Q, of analyte is provided. The collection efficiency of this configuration is a function of Peclet number, based on channel height, H, the average velocity, U_{ch}, and diffusivity, *Diff* as $Pe_{ch}=U_{ch}H/Diff$ [6]. When expressed in terms of flowrate, Q, the height dependence vanishes, $Pe_{ch}=Q/(LDiff)$.

The second case is the flow-through nanohole array with the same active sensing area as in the first case, provided the same solution at the same volume flow rate. The active sensing area of a nanohole array is the inner hole surface [4], and thus the number of nanoholes required for equivalent area is $N=L^2/A_{active}$, where the active area for a nanohole of diameter, D, and gold thickness, L_{hole}, is $A_{active}=\pi DL_{hole}$. The resulting number of holes is $N=L^2/\pi DL_{hole}$. The total flow rate is divided between these holes, resulting in an in-hole average velocity of $U_{hole}=U_{ch}(H/L)(4L_{hole}/D)$. Since the diameter of the hole and the thickness of the gold are typically similar (L_{hole} ~ 100 nm is thick enough to be optically opaque but thin enough to mill through, and D ~ 260 nm is small enough to prevent excessive direct transmission, and large enough to mill), the latter bracketed term is a small correction, on the order of 1. Since the diameters of the holes, D, and the thickness of the gold, L_{hole}, are typically similar, the average velocity in the channel with the microfluidic SPR sensor is roughly equivalent to that inside the nanoholes (for the case of L ~ H). The resulting Peclet number in the nanoholes is given by

$$Pe_{hole}=\frac{U_{hole}D}{Diff}=\frac{4QL_{hole}}{L^2Diff} \quad (9)$$

In both the microfluidic SPR sensor and the flow-through nanohole case, the Peclet number provides a measure of collection efficiency. Thus, the ratio of Peclet numbers provides a measure for comparison as follows:

$$\frac{Pe_{ch}}{Pe_{hole}}=\frac{QL^2Diff}{4QL_{hole}LDiff}=\frac{L}{4L_{hole}} \quad (10)$$

Equation (10) indicates that for the channel-based surface sensor to have comparable performance as the nanohole, it must be a sensor on the scale of a single nanohole, i.e. a channel with hydraulic diameter on the order of a single nanohole. Such a sensor would not be practical both because the analyte throughput, equivalent to a single nanohole, would be too low. Furthermore it is not possible to interrogate such a small area with traditional SPR. SPR spots must be larger than L ~ 40 μm to generate sufficient signal, and nanohole depths, L_{hole} ~ 100nm, are fixed by optical and fabrication considerations. These geometric contraints indicate a minimum Peclet number ratio of 10^2. In other words, given the same flow rate and active area, the Peclet number for the nanohole array is at least two orders of magnitude less than a typical microfluidic SPR sensor operating on otherwise similar conditions. The above scaling analysis suggests that nanohole array based sensing can achieve effectively complete collection, or sieving of analytes in cases were tradiational microchannel based surface sensors collect comparably few analytes, under otherwise similar conditions.

To provide a more detailed analysis of the transport in both cases, a computational model is employed. In these simulations, the binding kinetics are assumed to be perfect and the surface concentration is set to $c_S(t)=0$. This simplification allows the transport characteristics of the two systems to be compared in isolation from surface binding kinetics (finite surface reaction rates are introduced in results that follow). The steady state analyte concentration is solved in both a microscale SPR sensor with dimensions typical of commercial systems, such as Biacore (GE Health Sciences) with L = 100 μm, and a single representative nanohole from a flow-through nanohole array (with D = 300 nm a gold thickness of L_{hole} = 100 nm, and 10^5 nanoholes for equivalent active area).

Figure 3a shows the results of the steady state simulations with perfect reaction kinetics for the case of Q = 10 nl/min was provided to both systems. In the microfluidic SPR case, the depletion region is thin compared to the channel width and as a result the majority of target molecules are swept downstream before they can diffuse to the active sensing area. In the nanohole flow-through case, the depletion zone extends across the entire nanohole cross section, achieving effectively complete collection of analytes. Specifically, the Peclet number in the nanohole was, Pe_{hole} = 3, which resulted in 90% collection efficiency, as compared to the case of the microchannel sensor with $Pe_{ch}=10^3$, which resulted in only a 2% collection efficiency. Thus the sieving action of the nanohole array sensor captures 90% all the incoming analyte while 98% of the analyte totally bypasses the microfluidic SPR

system. It is important to note that given a specific flow rate, reducing the channel height would not change the Peclet number in the channel and thus not improve the collection efficiency. The only practical solution to improve the collection efficiency in the microfluidic SPR sensor case would be to decrease the flowrate by a factor of 300, at the cost of decreasing through-put and response time by the same factor.

Figure 3b indicates the sieving capacity of nanoholes with surface flux plotted versus flowrate, non-dimensionalized as dimensionless flux versus Peclet number. The diagonal line corresponds to effectively complete collection of analyte. The nanohole array sensor achieves effectively complete (i.e. > 99 %) collection operating at $Pe_{hole} \sim 1$ or below.

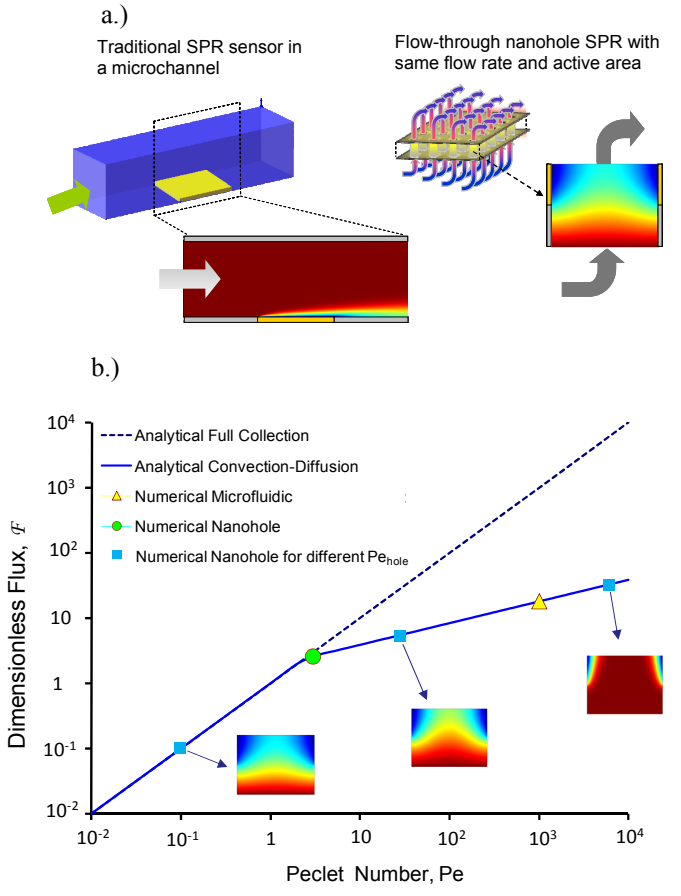

Figure 3. (a) Schematics of the two comparison cases, microfluidic channel with Microfluidic case (left) and flow-through Nanohole case (right). Simulation results comparing the analyte collection of a microfluidic SPR sensor (L = 100 μm) in a microchannel, and a flow-through nanohole (D = 300 nm, L_{hole} = 100 nm) array of equivalent active area given the same flow rate (Q = 0.6 μL/min) for the transport-only case (i.e. no reaction kinetics included, *cs(t)* = 0). The nanohole array sensor captures 90% of the analyte, as compared to 2 % collection in the microfluidic sensor case. (b) Extension of results shown in a with dimensionless flux versus Peclet number. Dashed line indicates full collection limit. Sample computational results shown inset and microchannel and nanohole cases from a are indicated as in the legend.

A corresponding microfluidic SPR system with $Pe_{ch} \sim 10^2$ would collect only ~10% of analyte. The two specific cases shown in Figure 3a are indicated by the circle and triangle in Figure 3b. In summary, enhanced transport in flow-through nanohole arrays makes it possible to achieve effectively complete analyte collection at flowrates compatible with typical sensing schemes (~ 10nL/s). At similar flow rates traditional microfluidic SPR sensing would sample only a fraction of the analyte stream, regardless of binding kinetics.

Finite binding kinetics, in general, have the effect of slowing down sensor response as compared to the purely transport limited case. In this context it is informative to determine the kinetic conditions under which the flow-through nanohole array strategy is beneficial, and the conditions under which it provides negligible benefit. Towards this end, binding kinetics were included in the model for both the microchannel and the nanohole test case systems.

In order to characterize the kinetic binding systems in as general and widely applicable way as possible, the characteristic binding timescale τ from equation 7 is employed.

Figure 4 shows the response time for both the flow-over (i.e. microfluidic SPR) as compared to the flow-through configuration for four different test cases. The response time is taken as the time for the sensor to have 80% of the equilibrium analyte concentration adsorbed to the surface. Details of the binding kinetics for each test case are provided in Table 1. Case 1 represents the binding of a molecule such as Bovine Serum Albumin (BSA) [15] and Case 2 is modelled after the antigen-antibody binding kinetic parameters of the cancer biomarker CA125 [16]. Case 3 represents a small molecule bioassay with relatively fast "on" kinetics, whereas case 4 represents the same case but with a less favorable kinetics. As indicated in Table 1, the binding kinetics for Case 1 (BSA) give a binding time constant of ~ 100 s (i.e. in the limit of perfect transport). Figure 4 shows that with the flow-through nanohole the response time is approximately equivalent to τ, indicating that the near-perfect transport limit is achieved. For the microchannel SPR case the sensor response is ~ 8 times slower. The flow-through strategy also provides much faster response when applied to the analyte system of Case 2 (CA125 cancer biomarker). For Case 3, however, the benefit of the flow-through nanohole approach is less significant. This is due to a combination of the smaller molecular size (increasing the diffusive transport rate in both cases) and the much slower (i.e. rate limiting) binding kinetics as indicated by the large characteristic τ value. Case 4 represents a further extreme, where binding kinetics limit the process entirely. The flow through strategy provides a faster response, however, the time savings are not significant as compared to the long characteristic binding time (τ = 10,000s). As illustrated by these cases, binding kinetics apply a minimum timescale for system response (i.e. a perfect transport limit).

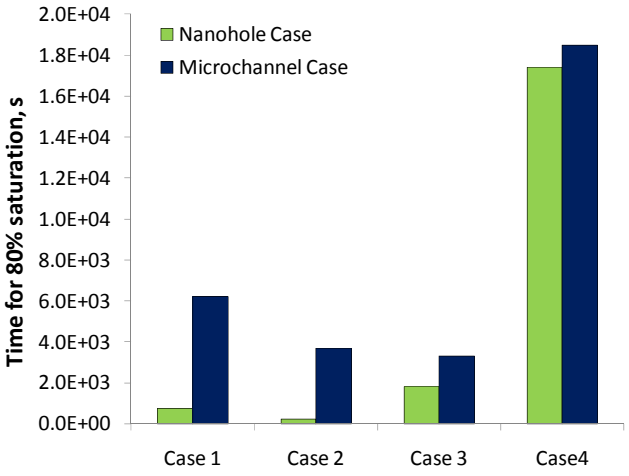

Figure 4. Time required for 80% of saturation of the active surface of the sensor for different cases.

Nanohole arrays improve transport in all cases; however, the benefit is not significant in systems constrained by slow binding kinetics.

Figure 5 provides time response as a function of the mass transport timescale spanning five orders of magnitude. In the simulations, the adsorption constant was varied as $1x10^2 \leq k_{on} \geq 1x10^7$ $M^{-1}s^{-1}$, keeping constant values of $k_{off} = 1x10^{-8}$ s^{-1}, c = $1x10^{-6}$M, and Q = 2µl/min. In all cases, the bulk concentration was higher than the dissociation constant $K_D = k_{off}/k_{on}$ to guarantee the effective saturation of the sensor. In these cases, equilibrium is reached by means of the "on" kinetics and the "off" kinetics are rather irrelevant. This is representative of many bioassays, having k_{on} values in the range of 10^3 to 10^5 $M^{-1}s^{-1}$ and k_{off} values ~ 10^{-3} s^{-1} [17]. As shown in the figure, the flow-through nanohole system provides maximum benefit at low τ values where mass transport presents the only limitation. As τ increases binding kinetics become dominant (first for fast diffusing species and later for slow diffusing species) all response curves asymptotically approach the mass transport limit (t = τ).

Figure 6 provides the results of Figure 5 in terms of improvement ratio, which is defined as the % improvement of response time. As shown, a benefit of 2000%, or 20-fold, is achieved for small (rapidly diffusing) analytes in the fast reaction limit. As the binding timescale increases, the benefit decreases.

Table 1. Diffusion coefficient, adsorption constant, desorption constant and characteristic binding timescale for cases 1-4 plotted in Figure 3.

	Case 1	Case 2	Case 3	Case 4
D (m^2s^{-1})	$1x10^{-11}$	$1x10^{-10}$	$1x10^{-9}$	$1x10^{-9}$
k_{on} (m^3s^{-1} mol^{-1})	$1x10^4$	$2x10^6$	$1x10^3$	$1x10^2$
k_{off} (s^{-1})	$1x10^{-4}$	$2x10^{-3}$	$1x10^{-7}$	$1x10^{-8}$
τ (s)	$1x10^2$	0.4	$1x10^3$	$1x10^4$

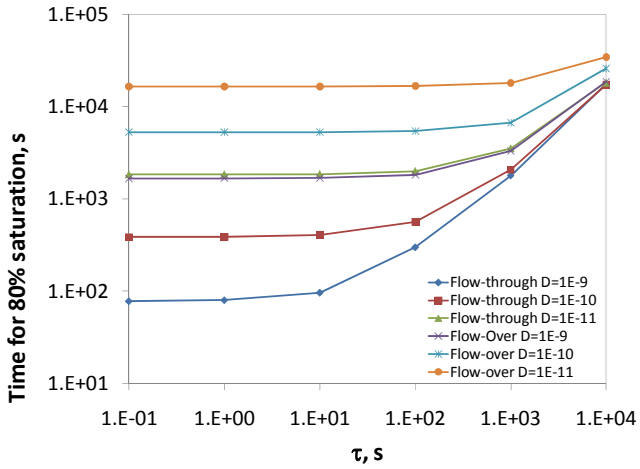

Figure 5. Time required to achieve 80% of saturation of the available binding sites on the active area of the sensor as a function of the binding kinetics time constant. Results for three different diffusion coefficents cases are plotted for both the flow-through and flow-over cases.

These results indicate that a significant benefit (i.e. > 200% improvement in response time) is achieved for cases with binding time constants up to 10^3 s. Most biosensor applications employ analytes with binding time constants in the range of 1 s to 10^2 s [10, 15, 17-19]. In that range, flow through nanohole array sensors can provide ~ 10-fold improvement in response.

5. CONCLUSION AND RECOMMENDATIONS

In this work, the collection efficiency and time response of flow-through nanohole arrays is quantified and compared with a traditional surface based sensor in a microchannel. The application of a scaling analysis and the computational model to the case of infinitely fast surface reaction provided a measure of transport characteristics of both systems.

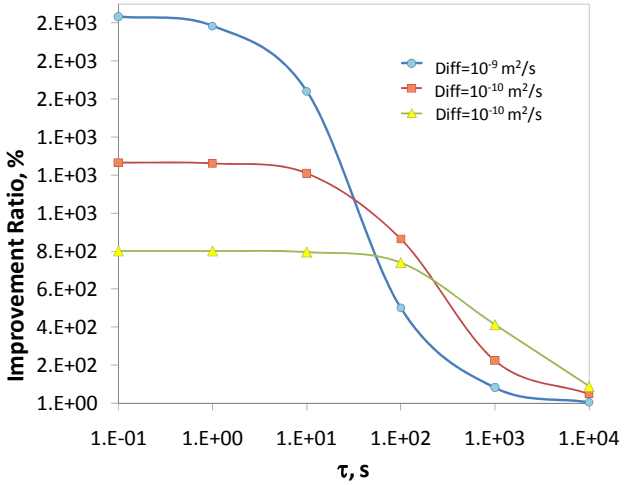

Figure 6. Improvement ratio of flow-through compared to flow-over.

The scaling analysis indicated that the nanohole array exhibits a Peclet number (which dictates cross-stream diffusive mass transport) 10^2 fold less than the microchannel case for the same given flow rate. Computational results support this finding. For instance, given the same flow rate (Q = 10 nL/min) for the transport-only case (i.e. no reaction kinetics included, cs(t) = 0). The nanohole array sensor captures 90% of the analyte, as compared to 2 % collection in the microfluidic sensor case. Finite binding kinetics, in general, have the effect of slowing down sensor response as compared to the purely transport limited case. Binding kinetics were included in the model for both the microchannel and the nanohole test case systems, and the system response times were compared as a function of binding time constant and diffusion coefficient.

A benefit of 2000%, or 20-fold, is achieved for small (rapidly diffusing) analytes in the fast reaction limit. With slower binding timescales the benefit is reduced. In the range applicably to most biosensing applications (τ = 1 to 10^3 s), and analytes with typical diffusion coefficients (D ~ 10^{-10} m^2/s), flow-through nanohole arrays offer ~ 10-fold benefit over established microfluidic sensors.

NOMENCLATURE

A_{active}	=	Active sensing area, m^2
b_0	=	Surface concentration of receptors, mol/m^2
c_0	=	Concentration of bulk fluid, M
c_S	=	Surface concentration of adsorbed species, mol/m^2
D	=	Nanohole diameter, m
Diff	=	Diffusivity, m^2/s
D_S	=	Surface diffusivity, m^2/s
H	=	Microchannel height, m
k_{on}	=	Adsorption kinetic constant, $M^{-1}s^{-1}$
k_{off}	=	Desorption kinetic constant, s^{-1}
L	=	Microchannel active area length, m
L_{hole}	=	Nanohole active area length, m
Q	=	Flow rate, m^3/s
Pe_{ch}	=	Peclet number in the microchannel
Pe_{hole}	=	Peclet number in the nanohole
t	=	Time, s
U_{ch}	=	Fluid velocity in the microchannel, m/s
U_{hole}	=	Fluid velocity in the nanohole, m/s

Greek

τ	=	Equilibration time, s

ACKNOWLEDGMENTS

The authors gratefully acknowledge the financial support of the Natural Sciences and Engineering Research Council of Canada, NSERC.

REFERENCES

[1] T. W. Ebbesen, H. J. Lezec, H. F.Ghaemi, T. Thio, P. A. Wolff, Nature, 391, 667–669 (1998).
[2] C. Genet, T. W. Ebbesen, Nature 2007, 445, 39–46
[3] W. L. Barnes, A. Dereux, and T.W. Ebbesen, Nature 424, 824-830 (2003).
[4] R. Gordon, D. Sinton, K. L. Kavanagh and A. G. Brolo, Accounts of Chemical Research, 41, 1049-1057, (2008).
[5] K.A. Tetz, L. Pang, and Y. Fainman, Optics Letters 31, 1528-1530 (2006).
[6] J. Ferreira, M. Santos, M. Rahman, A. G. Brolo, R. Gordon, D. Sinton, Girotto, E. J. Am. Chem. Soc., 131, 436-437 (2009).
[7] F. Eftekhari, C. Escobedo, J. Ferreira, E.M. Girotto, A.G. Brolo, R. Gordon, D. Sinton, Analytical Chemistry 81, 4308-4311 (2009).
[8] T. M. Squires, and S. R. Quake, Rev. Mod. Phys., 77, 977-1026 (2005).
[9] J. A. Goodrich and J. F. Kugel, Binding and kinetics for molecular biologists, Cold Spring Harbor Laboratory Press, Cold Spring Harbor, N.Y., 2007.
[10] G. Hu, Y. Gao, and D. Li, Biosensors and Bioelectronics, 22, 1403-1409 (2007).
[11] I. Chaiken, S. Rose, R. Karlsson, Anal. Biochem. 201, 197–210 (1992).
[12] Myszka, D.G., He, X., Dembo, M., Morton, T.A., Goldstein, B., Biophys. J. 75, 583–594 (1998).
[13] T. Gervais, and K. F. Jensen, Chem. Eng. Sci. 61, 1102-1121 (2006).
[14] T.M. Squires, R.J. Messinger, and S.R. Manalis, Nature Biotech, 26, 417-426 (2008).
[15] N. Meechai, A. M. Jamieson, and J. Blackwell, J. Colloid and Int. Sci., 218, 167-175 (1999).
[16] C. Xie, C. Dong, J. Ren, Talanta, 79, 971-974 (2009)
[17] E. Laffly1, T. Pelat1, F. Cédrone, S. Blésa, H. Bedouelle, and P. Thullier, J. Mol. Biol., 378, 1094-1103 (2008).
[18] Y. L. Gao, G. Q. Hu, F. Y. H. Lin, P. M. Sherman, and D. Q. Li, Biomed. Microdevices, 7, 301-312 (2005).
[19] X. Zhang, M. A. Young, O. Lyandres, and R. P. Van Duyne, J. Am. Chem. Soc., 127, 4484-4489 (2005).